# The influence of increased air flow on the spatial variation of iron sinter quality

by A.M. Garbers-Craig, J.M.A. Geldenhuis, W.J. Jordaan, and P.C. Pistorius*


## Synopsis

The aim of this investigation was to study the influence that varying production rates have on iron sinter quality. This was done by performing sinter pot tests at different pressure drops over the sinter bed, namely 11 kPa and 15 kPa (for 500 mm total bed depths). During each of the sintering processes temperature-time profiles were recorded of the top, middle and bottom layers of the sinter bed. On completion of the sinter process the sinter cakes were divided into top, middle and bottom layers. The physical properties of each layer were subsequently characterized by performing a tumbler test and a sieve analysis. A comprehensive mineralogical study was also conducted on each layer.

This study revealed that sinters of similar cold strength could be produced under the examined production rates. However, a higher production rate was accompanied by an increased amount of fines.

The cold strengths of both sinters significantly increased from the top layer to the bottom layer of the sinter bed. This strength variation is not related in any simple way to the phase composition.


Keywords: Sinter, sinter bed, production rate, phase composition, cold strength, tumbler index, sieve analysis, temperature-time profile

## Introduction

It is well known that the quality of sinter is mainly governed by the microstructure and phase composition of the sinter. However, as sintering conditions are not uniform throughout the sinter bed, the phase composition, and therefore the sinter quality, vary in the sinter bed. From a production point of view it is important to optimize the sintering process with regard to both sinter quality and the production rate. The aim of this investigation was therefore to investigate the influence that different production rates would have on sinter quality. This was done by monitoring the temperature-time profiles in the sinter bed when different air flow rates were used, and relating these profiles to the strength of the sinter, the amount of fines produced and its total magnetite, SFCA and glass contents.

## Background

### *Sintering mechanism*

The sintering mechanism is briefly reviewed to facilitate interpretation of the phase compositions, which are reported later in this paper.

Iron ore granules, which are charged to the sinter bed, consist of a large iron ore core particle with an adherent coating of fines. The layer of fines consists of highly reactive ore particles, fluxes and other raw materials that are in intimate contact. It is assumed that the sintering reactions begin within the layer of adhering fines[1].

Combustion of fine coke particles starts at temperatures between 700°C and 800°C and results in the formation of CO gas. The surface of the iron ore core and its adhering fines are reduced to magnetite. As the temperature rises to 1100°C , low melting point phases such as $Fe_2O_3$-CaO, FeO-CaO and FeO-$SiO_2$ are formed by solid-solid reactions[2-3]. The phase termed SFCA (silico-ferrite of calcium and aluminium), forms in association with magnetite. Acicular SFCA starts to form below 1185°C; when the temperature has risen to 1245°C the unreacted hematite has disappeared and the SFCA crystal size increases[3]. The SFCA begins to decompose when the temperature exceeds 1300°C[2,3]—forming hematite if the partial pressure of oxygen is high and the temperature is lower than 1350°C, and magnetite when the partial pressure of oxygen is low and the temperature is higher than 1350°C; the slag components are redistributed into the melt. Decomposition of SFCA is enhanced by extended time above the decomposition temperature, and increased maximum temperature.

* *Department of Materials Science and Metallurgical Engineering, University of Pretoria, Pretoria 0002.*

 *SA ISSN 0038–223X/3.00 + 0.00. Paper received Apr. 2003; revised paper received Aug. 2003.*

Magnetite precipitates on subsequent cooling, and SFCA re-precipitates at lower temperatures, after magnetite and hematite[4]. Both hematite and magnetite can be resorbed by reaction with the silicate melt to form SFCA (favoured by slow cooling).

### *Sinter quality*

Sinter quality refers to the physical and metallurgical properties of the sinter. The quality of sinter is usually defined in terms of:

- The physical strength of the sinter at room temperature as measured by the shatter or tumbler test
- The breakdown of sinter following reduction at low temperatures (550°C) determined by the reduction degradation test (RDI)
- The reducibility of the sinter determined by the reducibility test (RI) at 900°C
- The high temperature softening and melting properties of the sinter.

All of these properties are governed by the microstructure of the sinter, in particular the bonding phases—notably SFCA—that make up the majority of phases within sinter (up to 80 vol%)[2,3,5,6].

### *Temperature-time characteristics of sintering*

From the discussion on the sintering mechanism it is clear that the sinter phases are mainly formed during the sinter process at temperatures above 1100°C. Therefore, the temperature-time characteristics of the sinter process contribute strongly to the microstructure and phase composition of sinter.

The temperature profile in the sinter bed is characterized by a steep rise to a maximum temperature ($T_{max}$) during the heating cycle[7]. The maximum temperature reached is often higher than 1300°C and may be as high as 1350°C[8]. A gentle slope after reaching maximum temperature indicates the relatively slow cooling of the finished sinter during the cooling cycle.

Due to changes in bed permeability during the sintering process, different temperature profiles are obtained from top to bottom in the sinter bed. Therefore, the heating rate, maximum temperature reached, time at temperatures higher than 1100°C and the cooling rate will differ in the top, middle and bottom layer of the sinter bed[9]. Due to the different temperature-time characteristics there will be a variation in the phase composition through the sinter bed. Because of these differences the sinter may be classified as follows[10]:

***Top sinter:*** generally weak and friable giving a poor yield of sinter with an acceptable size grading. This sinter is fused at a high temperature and chilled immediately thereafter. The sinter is discharged cold from the sinter strand.

***Middle sinter:*** This sinter is formed under optimum conditions for fusion and annealing and gives the maximum yield of sinter with acceptable size grading. The sinter is discharged cold from the sinter strand.

***Bottom sinter:*** This sinter is discharged hot and is chilled severely as it passes through the breaker and over the discharge screen onto the cooler. This may result in poor physical properties giving a lower yield of sinter with acceptable size grading. If on-strand cooling applies, the sinter will have almost the same properties as the sinter in the middle layer.

*Table I*

**Chemical composition (mass percentages) of sinter**

| | |
|---|---|
| FeO | 6.58 |
| $Fe_2O_3$ | 67.90 |
| CaO | 12.33 |
| MgO | 2.73 |
| $SiO_2$ | 6.01 |
| $A1_2O_3$ | 2.03 |
| $K_2O$ | 0.06 |
| $Na_2O$ | 0.03 |
| MnO | 1.30 |
| $TiO_2$ | 0.13 |
| P | 0.07 |
| S | 0.02 |
| C | 0.24 |

### Experimental procedure

Experiments were designed to investigate the effect of increased production rate on sinter quality. The experiments were performed with a sinter pot, using as feed a mixture based on that used at a South African integrated steel plant. The sinter mixture contained a mixture of three iron ores, 29% return fines and 9.8% waste oxides, 5.5% water and 3.2% coke by mass, and sufficient lime and dolomite to obtain the required basicity ($CaO/SiO_2 = 2$). The dry raw materials were mixed together in a rotary mixer. The water was added and further mixing for six minutes resulted in adequate granulation.

The sinter pot was lined with a grid layer (50 mm deep) consisting of -40+20 mm sinter particles, on top of which the mixture was placed. The total sinter bed height was 500 mm. The average chemical composition of the produced sinter is shown in Table I.

During the sinter pot tests, the main controlled variable was the pressure drop across the bed. The sinter pot had a cross-sectional area of 0.16 $m^2$.

The surface of the mixture was ignited with a gas flame under a pressure drop of 5 kPa over the bed. The ignition temperature measured on the surface of the sinter bed was 1000°C. After an ignition time of 1.5 minutes the gas flame was extinguished and the pressure drop over the sinter bed was increased to the relevant test pressure drop. In the first series of sinter pot tests the pressure drop was increased to 11kPa. To increase the air flow rate the pressure drop over the sinter bed was increased to 15 kPa during the second series.

During tests, the off-gas flow rate was measured at the outlet of the sinter pot. The temperature profiles in the sinter bed were determined with three thermocouples, which were distributed vertically at equal intervals. These K-type thermocouples were inserted into the sinter bed before the sinter was ignited by the gas flame. The off-gas temperature was monitored with a thermocouple placed directly below the sinter bed.

Each sinter cake obtained from the sinter pot tests was physically divided into three layers to form a top layer, middle layer and bottom layer. The different layers of both series were separately prepared for mineralogical and physical evaluation. Three lots of sample were prepared for each set of conditions to obtain sufficient material for physical characterization. This yielded about 70 kg of material from the top layer, 85 kg from the middle layer, and 140 kg from the bottom.

The physical properties of the sinter in each layer of both series were characterized by the sieve analysis and the resistance to degradation by impact and abrasion at room temperature, as determined with the ISO 3271 tumbler strength test.

Samples from each layer were prepared for ICP analysis, point counting (1 000 points were counted per sample) and microprobe analysis (using WDS).

## Results and discussion

### *Effect of pressure drop on air flow rate, sintering time, and temperature profiles*

The measured temperature histories within the sinter bed and gas flow rates through the sinter bed are shown in Figure 1. (The gas flow rates as shown in the figure were measured just before the fan, where the gas had cooled to approximately 30°C.) During the first part of the sintering cycle (following ignition) the permeability of the sinter bed decreased due to the sintering reaction and formation of the melt, and the air flow rate decreased to a minimum (see Figure 1 and Table II). At this stage the temperature reached a maximum in the top layer. Towards the end of the sintering cycle the permeability of the sinter bed increased (due to solidification of the phases), resulting in increased air flow. The sintering cycle was taken to have ended when the off-gas temperature started to decrease. Figure 1 shows that this time corresponded approximately to the time at which the temperature peaked in the lower layer of the sinter bed.

The sinter was cooled in the sinter pot during the cooling cycle. During this period, the air flow rate was higher than during the preceding sintering process (Figure 1). The cooling cycle was taken to have ended when the off-gas temperature reached 150°C.

The speed of downward movement of the reaction zone is a function of the airflow rate. Figure 1 (b) illustrates the much shorter sintering time when the pressure drop was increased to 15 kPa (giving a higher average air flow rate) (see also Table II). However, the peak temperature was unaffected by the air flow rate.

The temperature-time characteristics in each layer are summarized in Table III. Heating and cooling rates were determined from tangents to the temperature curves at 700°C (on the rising and falling sections respectively). Clearly, the heating and cooling rates were only slightly larger with the higher air flow rate, and the major thermal effect of the higher gas flow rate was a decrease in holding time at elevated temperature (Table III). The residence time above

*Table II*

**Gas flow rates during the sintering and cooling cycle, for Series 1 and Series 2 tests**

| | | Series 1 | Series 2 |
|---|---|---|---|
| **Sintering cycle** | | | |
| Pressure drop over sinter bed | kPa | 11 | 15 |
| Gas flow after ignition sequence | l/minute | 4062 | 5389 |
| Minimum gas flow rate | l/minute | 2115 | 4237 |
| Gas flow at end of sintering cycle | l/minute | 4069 | 7174 |
| Average gas flow rate | l/minute | 2983 | 5194 |
| Duration of sintering cycle | minutes | 21 | 16 |
| Maximum off-gas temperature | °C | 417 | 366 |
| **Cooling cycle** | | | |
| Pressure drop over sinter bed | kPa | 11 | 15 |
| Average gas flow rate | l/minute | 6629 | 9723 |
| Duration of cooling cycle | minutes | 21 | 15 |
| **Total sintering time** | minutes | 42 | 31 |

*Table III*

**Temperature-time characteristics**

| Parameter | Top | Middle | Bottom |
|---|---|---|---|
| **Series 1: 11kPa** | | | |
| Heating rate [°C/s] | 11 | 11 | 13 |
| T maximum [°C] | 1393 | 1391 | 1391 |
| Cooling rate [°C/s] | 2.0 | 1.9 | 1.7 |
| Time at T>1100°C [min] | 9.3 | 9.8 | 9.6 |
| | | | |
| **Series 2: 15 kPa** | | | |
| Heating rate [°C/s] | 13 | 11 | 19 |
| T maximum [°C] | 1402 | 1393 | 1391 |
| Cooling rate [°C/s] | 2.6 | 2.2 | 2.1 |
| Time at T>1100°C [min] | 6.3 | 6.4 | 6.2 |

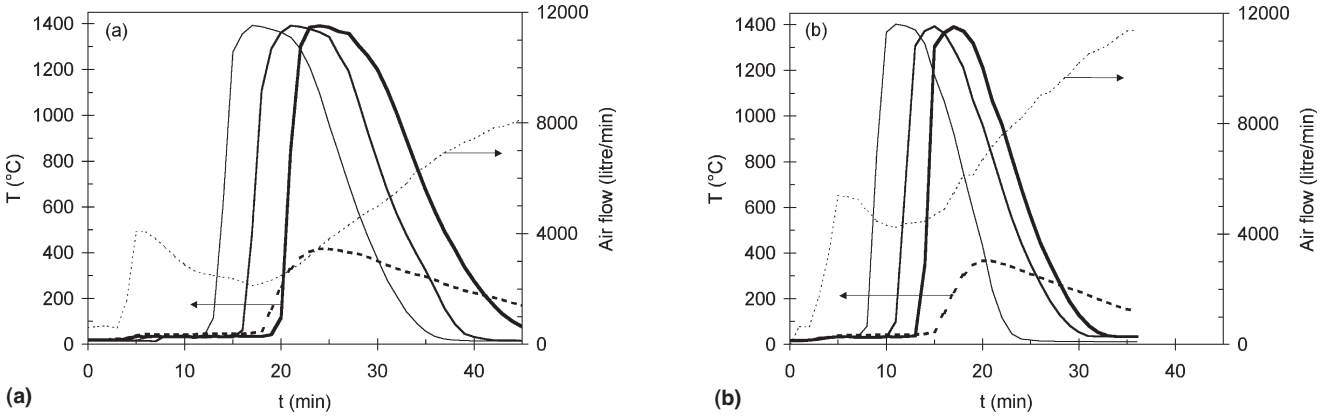


**Figure 1—Variations in bed temperature and gas flow through a 500 mm deep sinter bed, with pressures drops of respectively (a) 11 kPa and (b) 15 kPa across the bed. Solid lines give the temperature histories at points in the upper middle and lower parts of the bed respectively; the thinner broken line indicates the gas flow rate, and the heavier broken line the off-gas temperature**

1100°C is considered significant because phase formation occurs in this temperature region; it is assumed that the sintering process is complete when the temperature drops below 1100°C[3]. Therefore, the longer the residence time in this temperature region the more time there will be for phase formation. This may result in the formation of a higher content of phases (such as SFCA) that enhance sinter quality.

### *Phase composition of the sinter*

This study revealed that the main constituents of the produced sinter are hematite, magnetite and SFCA, with small quantities of calcium silicate, glass, periclase, wustite and manganosite. The volume percentages of these phases, as determined by point counting, are given in Table IV. The volume percentages of the main phases are also presented in Figure 2.

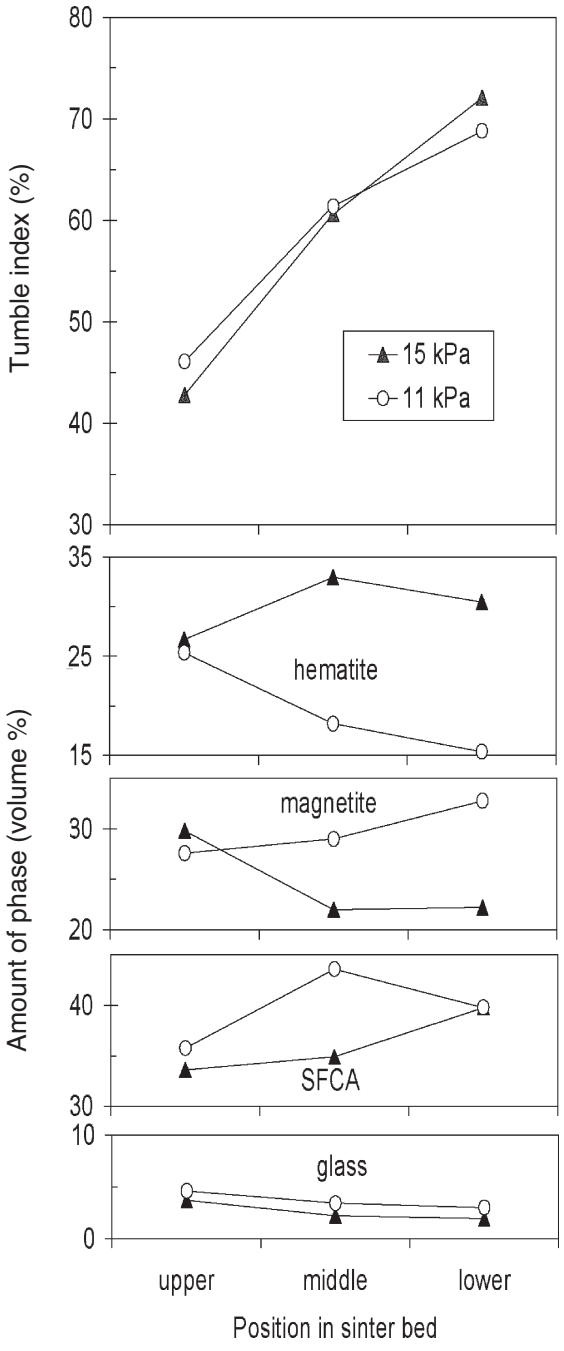


**Figure 2—Physical properties and phase compositions of sinters. The top pair of graphs shows the changes in tumble index (fraction of material remaining larger than 6.35 mm in diameter after simulated handling), and the lower four sets of graphs show the phase composition. 'Upper', 'lower' and 'middle' refer to the different positions within the sinter bed. The data for the pressure drop of 11 kPa are indicated by open circles, and those for 15 kPa by filled triangles**

### *Hematite*

Three types of hematite commonly occur in this sinter. Massive hematite particles resemble the original hematite particles added to the raw materials mixture. These particles were only partially affected during sintering. In all the layers massive hematite dominates as the main hematite phase (between 47 and 79% of the total hematite). An example of the microstructure containing massive hematite is shown in Figure 3.

Some of the massive hematite particles display recrystallized outer rims (Figure 3). The crystalline hematite occurs as euhedral to subhedral as well as skeletal and/or dendritic

*Table IV*

**Phase analysis of the sinters**

| Sinter phase | Series1: 11 kPa | | | Series 2: 15 kPa | | |
|---|---|---|---|---|---|---|
| Vol% | Top | Middle | Bottom | Top | Middle | Bottom |
| Magnetite | 27.60 | 29.00 | 32.80 | 29.80 | 22.00 | 22.20 |
| Massive hematite | 18.60 | 8.60 | 8.60 | 19.40 | 26.00 | 23.60 |
| Crystalline hematite | 6.60 | 9.00 | 6.60 | 7.20 | 6.90 | 6.70 |
| Secondary hematite | 0.20 | 0.60 | 0.20 | 0.10 | 0.10 | 0.20 |
| Total hematite | 25.40 | 18.20 | 15.40 | 26.70 | 33.00 | 30.50 |
| Columnar SFCA | 5.80 | 10.80 | 8.40 | 3.00 | 4.00 | 7.30 |
| Acicular SFCA | 24.60 | 28.80 | 26.40 | 25.80 | 26.50 | 30.20 |
| Dendritic SFCA | 5.40 | 4.00 | 5.00 | 4.80 | 4.40 | 2.30 |
| Total SFCA | 35.80 | 43.60 | 39.80 | 33.60 | 34.90 | 39.80 |
| Ca-silicate | 3.00 | 5.00 | 6.80 | 3.40 | 3.10 | 3.30 |
| Glass | 4.60 | 3.40 | 3.00 | 3.70 | 2.20 | 1.90 |
| Periclase | 2.40 | 0.60 | 2.00 | 1.80 | 3.80 | 1.20 |
| Wustite | 1.00 | 0.00 | 0.00 | 0.10 | 0.20 | 0.20 |
| Manganosite | 0.20 | 0.20 | 0.20 | 0.40 | 0.50 | 0.10 |

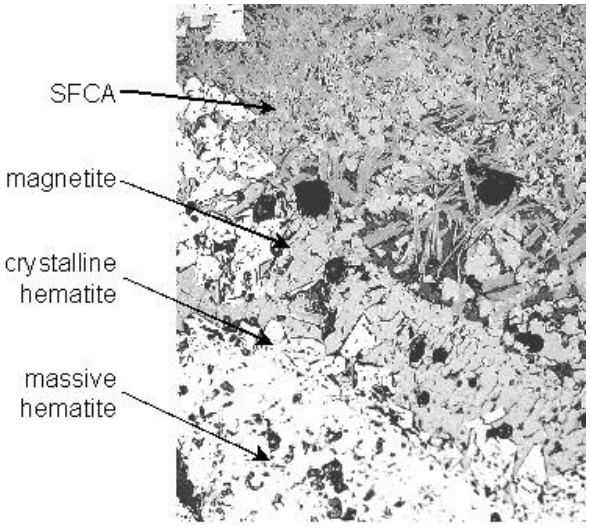


**Figure 3—Massive hematite displaying a recrystallized rim of crystalline hematite. The hematite is associated with euhedral to subhedral magnetite crystals embedded in a silicate-rich glassy matrix. Optical micrograph (X 200)**

hematite crystals, which crystallized during cooling of the sinter. Between 21 and 49% of the produced hematite is crystalline hematite that precipitated from the melt.

The remaining hematite consists of very small quantities of secondary hematite, which probably formed by re-oxidation of magnetite at high temperatures. Secondary hematite is usually bound in a matrix of calcium silicate and SFCA.

The massive hematite content (and therefore also the total hematite content) of the sinter in series one decreased from the top layer to the bottom layer. In series two, however, the massive hematite content increased from the top layer towards the bottom layer, but reached a maximum in the middle layer (Table IV). The total hematite content of series one (11 kPa) is lower than the total hematite content of series two (1 5 kPa) (Figure 2).

*Magnetite*

The magnetite is present as well-defined euhedral to subhedral crystals as well as skeletal and dendritic crystals. Magnetite crystals are present in close association with SFCA (Figure 4). The calculated stoichiometry of the magnetite in all the layers indicated that this phase is actually an iron rich spinel solid solution phase with an $(Fe,Mg,Mn)(Fe,Al)_2O_4$ stoichiometry. The magnetite content of series one increases from the top layer to the bottom layer, while in the case of series two it decreases towards the bottom layer (Table IV). The magnetite content therefore correlates inversely with the hematite content.

At the lower air flow (series one) the sintering time at temperatures above 1100°C was longer. It can therefore be expected that more hematite is reduced to magnetite in series one than in series two, due to the longer reaction times. Magnetite is also formed from the dissociation of SFCA at temperatures higher than 1300°C[2,3]. The proportion of SFCA that is decomposed may increase when the time of exposure above the decomposition temperature increases or when the maximum temperature that is reached during sintering increases. This could also explain why more magnetite was formed in series one than in series two, as longer sintering times prevailed above 1300°C.

*SFCA*

The SFCA (silico-ferrite of calcium and aluminium) phase is present as dendritic SFCA, acicular SFCA and columnar SFCA, depending on the size of the crystals. Dendritic SFCA is the first type of SFCA that forms during the sintering process[8]. These crystals are very small, usually smaller than 4µm (Figure 5). Between 6 and 15% of the total SFCA consist of dendritic SFCA. Crystal growth between 1200°C and 1300°C results in bigger crystals, larger than 4µm but smaller than 10µm, called acicular SFCA[8] (Figure 6). Acicular SFCA dominates as the main SFCA phase in all the layers (more than 66% of the total SFCA consists of acicular SFCA). At 1300°C acicular SFCA melts, and subsequently re-precipitates as columnar SFCA during cooling. These are rather large crystals with a typical size of 10µm and bigger[8]. Between 9 and 25% of the total SFCA is columnar.

The calculated stoichiometry of the SFCA in all the layers has the general formula of $Ca_5Si_2(Fe,Al)_{18}O_{36}$ or $M_{25}O_{36}$, which is the most commonly reported empirical formula for the SFCA phase.

In series one the highest total SFCA content is found in the middle layer and the lowest in the top layer. In series two, however, the total SFCA content increases from the top layer towards the bottom layer (Table IV and Figure 2). The total SFCA contents in the top and middle layers of series one are higher than that of series two. This could be due to longer sintering times at temperatures above 1100°C, although one would expect that longer sintering times above 1300°C would in turn enhance the decomposition of SFCA and therefore counteract an increase in SFCA content.

### *Physical properties*

The physical properties of the sinters were characterized by sieve analysis and the resistance to degradation by impact and abrasion at room temperature, as determined with the ISO 3271 tumbler strength test (Table V and Figure 2).

The results of the tumbler test indicate that there is no major difference between the cold strengths of the sinters

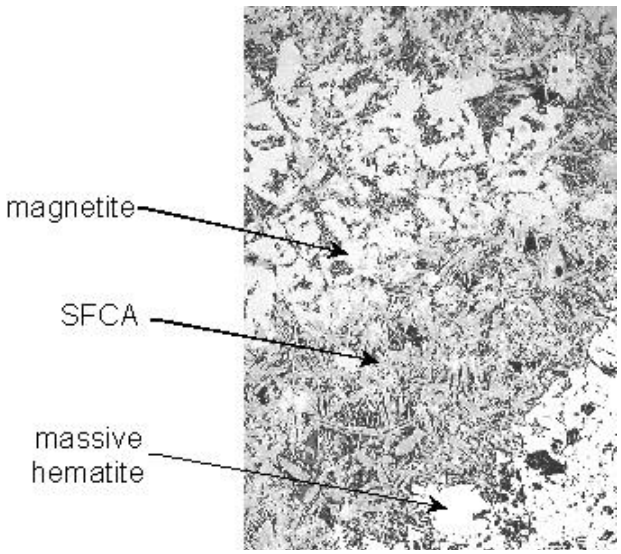


**Figure 4— Magnetite crystals embedded in a silicate-rich glassy matrix. The magnetite is in close association with SFCA crystals. Optical micrograph (X 200)**

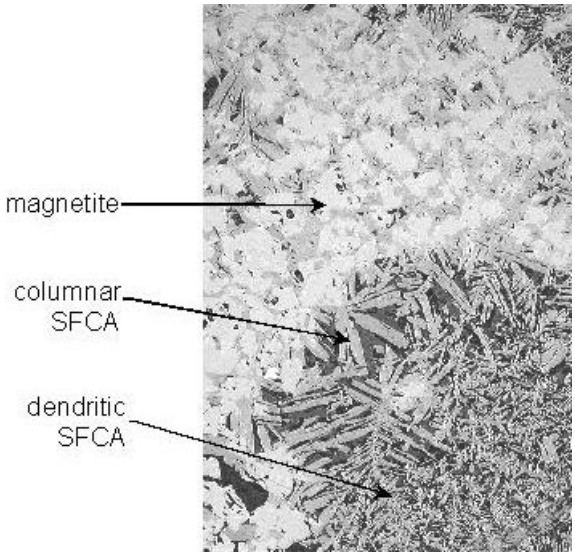


**Figure 5—Dendritic and acicular SFCA are the first types of SFCA that form during sintering. Crystal growth results in bigger crystals called columnar SFCA. Optical micrograph (X 200)**

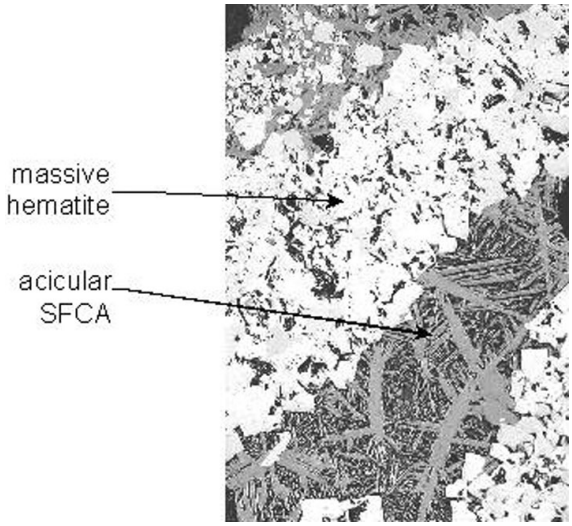


**Figure 6—Acicular SFCA in association with massive hematite. Optical micrograph (X 200)**

*Table V*
*Physical properties of the sinter*

| | Series1: 11kPa | | | Series 2: 15kPa | | |
|---|---|---|---|---|---|---|
| **Sieve analysis** | | | | | | |
| **mm** | **Top** | **Middle** | **Bottom** | **Top** | **Middle** | **Bottom** |
| **+40** | 1.40 | 6.23 | 14.90 | 0.00 | 2.55 | 5.01 |
| **-40+25** | 4.66 | 18.97 | 24.20 | 3.27 | 13.00 | 10.49 |
| **-25+16** | 18.72 | 27.30 | 24.53 | 12.56 | 29.73 | 19.15 |
| **-16+12.5** | 13.33 | 11.98 | 9.15 | 12.41 | 12.90 | 16.78 |
| **-12.5+10** | 11.60 | 7.75 | 6.60 | 12.52 | 9.47 | 11.49 |
| **-10+5** | 32.88 | 16.49 | 12.11 | 39.64 | 20.92 | 23.23 |
| **-5** | 17.42 | 11.27 | 8.52 | 19.59 | 11.43 | 13.85 |
| **Qualitative fractions** | | | | | | |
| **+16** | 24.78 | 52.50 | 63.63 | 15.83 | 45.28 | 34.65 |
| **-10** | 50.30 | 27.76 | 20.63 | 59.23 | 32.35 | 37.08 |
| **Mean particle size** | | | | | | |
| **mm** | 13.75 | 20.25 | 24.17 | 11.82 | 17.57 | 17.05 |
| **Tumbler test results** | | | | | | |
| **+6.30 mm** | 46.12 | 61.39 | 68.80 | 42.80 | 60.60 | 72.10 |
| **-6.30+0.50 mm** | 49.89 | 34.00 | 26.50 | 53.30 | 35.10 | 23.30 |
| **-0.50 mm** | 3.99 | 4.61 | 4.70 | 3.90 | 4.30 | 4.60 |

that were produced in the two series. The highest tumbler index is associated with the bottom layer of series 2. The effect of position within the sinter bed is much more significant than the effect of production rate, as Figure 2 clearly illustrates.

The results of the sieve analysis, together with two important size fractions (+16 mm and -10 mm), indicate that more fines are produced in series two than in series one, and that the quantity of fines decreases from the top layer towards the bottom layer.

The mean particle size of the sinter in series one is also larger than the mean particle size of the sinter in series two (Table V). The mean particle size of the top layer is also smaller than that of the middle and bottom layers in each series.

It can therefore be concluded that although the cold strengths of sinter produced in series one and two are similar, more fines were produced when production rates were higher.

### *Correlation between the quantity of phases formed and sinter quality*

Based on literature information, it is expected that the physical properties of the sinter should be directly affected by the relative amounts of the major phases. However, Figure 2 demonstrates that, for these tests, the phase composition was (unexpectedly) not a major influence: there was very little difference in the tumbler index of the two series, despite the clear and consistent differences in phase composition (which differences in phase composition were discussed above). Rather, the strongest effect by far was the spatial variation in sinter quality (through the thickness of the sinter bed).

While there are spatial differences in phase composition, the phase differences between the different vertical positions are generally smaller than the differences between the sinters produced at the higher and lower production rates (Figure 2): production rate has a larger effect on phase composition than does vertical position. In contrast, the major effect regarding sinter quality is the vertical positions within the sinter bed, and the production rate has a very minor effect (see Figure 2). This conclusion apparently disproves the hypothesis that the phase composition controls sinter quality; a surprising conclusion that is being investigated in further work. One likely origin of the spatial variation in sinter quality is differences in gross porosity.

## Conclusions

Increasing the airflow rate through the sinter bed significantly increases the production rate of sinter, without a loss in cold strength. The higher production rate did result in the formation of an increased amount of fines, however.

It was also found that the cold strength of the sinter, which was produced under the two selected production rates, significantly increases from the top layer to the bottom layer of the sinter bed. It appears that this difference in strength cannot be attributed unambiguously to differences in the amounts of phases. Other parameters such as morphology of the phases that are present in the sinter, and porosity, should also be investigated.

## References

1. Loo, C.E. *et al.* Influence of material properties on high-temperature zone reactions in sintering of iron ore. *Transactions of the Institute of Mining and Metallurgy,* 101, January-April. 1992. pp. C7–C16.
2. Sasaki, M. *et al.* Consideration on the properties of sinter from the point of view of sintering reactions. *Nippon Steel Corporation Tetsu-to-Hagane,* vol. 68. 1982. p. 563–598.
3. Dawson, P.R. Research studies on sintering and sinter quality. *Ironmaking and Steelmaking,* vol. 20. no. 2. 1993. pp. 17–143.
4. Dawson, P.R. *et al.* Influence of alumina on development of complex calcium ferrites in iron ore sinters. *Transactions of the Institute of Mining and Metallurgy,* 94, June. 1985. pp. C71–C78.
5. Bristow, N.J. and Waters, A.G. Role of SFCA in promoting high-temperature reduction properties of iron ore sinters. *Transactions of the Institute of Mining and Metallurgy,* 100, January–April. 1991. pp. C1–C10.
6. Mukherjee, T. *et al.* Structure of fluxed sinter. *Iron and Steelmaking* 1985. vol. 12, no. 4. pp. C151–C155.
7. Li-Heng H. *et al.* Sintering conditions for simulating the formation of mineral phases in industrial iron ore sinter. *ISIJ International.* vol. 29, no. 1. 1989. pp. 24–32.
8. Dawson, P.R. *et al.* The influence of the sintering temperature profile on the mineralogy and properties of iron ore sinters. *Proc. Australas. Inst. Min. Metall.* no. 289. June/July, 1984. pp. 163–169.
9. Li-Heng H. *et al.* Effect of oxygen potential on mineral formation in lime fluxed iron ore sinter. *ISIJ International.* vol. 29, no.8. 1989. pp. 625–634.
10. Davies, W. Some practical applications of fundamental sinter research. *Canadian Mining and Metallurgical Transactions,* vol. LXIII. 1960. pp. 114–126. ◆